Determination of Landmark Topography from Imaging Data

Robert W. Gaskell
MS 301/150
Jet Propulsion Laboratory
California Institute of Technology
4800 Oak Grove Drive
Pasadena, CA 91109
(818) 354-2116
rwg@piglet.jpl.nasa.gov

Abstract

Viking, MOC and MOLA data are being used to construst high resolution topographic and albedo models of landmarks on Mars. These models can be reilluminated and correlated with in-flight images, acting as body-fixed navigation tie-points. A similar procedure, using sparse stereo points in place of MOLA data, is being used to map small bodies such as Phobos and Deimos.

1. Introduction

Traditional optical navigation depends upon the imaging of a body of interest along with several stars in a single field of view. Since the stars are effectively infinitely far away, their locations in the image serve to determine the camera's orientation in inertial space. The known camera orientation, along with the nominal spacecraft trajectory and body ephmeris, enable the prediction of the body's image-space location. The residual between the nominal and observed image space location helps to update the knowledge of both the s/c trajectory and the body ephemeris.

As the spacecraft nears the body of interest, traditional opnav begins to fail. First, the body's brightness overwhelms the stars. Second, the body extends over a number of pixels, making centerfinding difficult. Finally, as the body fills the field of view, stars are completely obscured.

By the time the body covers perhaps a hundred pixels, individual surface features become visible. These features define landmarks, fixed points on the body's surface, that can be used like stars to determine the camera orientation and the body-relative camera (spacecraft) location [1].

Figure 1 shows a Viking orbiter image of Mars with a number of landmarks highlighted. The image has been processed to remove speckling and electronic distortion. Errors in camera pointing will result in a rigid shift or rotation of the pattern of landmarks. Errors in range will result in an expansion or contraction of the pattern. Finally, since the landmarks are at different distances, cross line-of-sight errors in camera location will result in a differential shift of the landmarks, with closer landmarks being shifted by a greater amount.

Figure 1. Processed Viking orbiter image 629A39 with landmarks

Since landmarks do not come equiped with little white squares to indicate their surface location, they must be defined in terms of the local topography and albedo variations surrounding the specified surface point. In particular, a landmark is presented as digital height and albedo maps in a local coordinate system with unit vectors in the south, east and vertical directions. The vector from the body center to the origin of the local coordinate system defines the landmark location.

Four such landmark patches are displayed in figure 2. Each is 50 kilometers square, 100 x 100 map pixels at 500 meter resolution. The resolution and pixel size can vary. They are determined by the intended application, but are also limited by the resolutions of the images used in the construction of the maps.

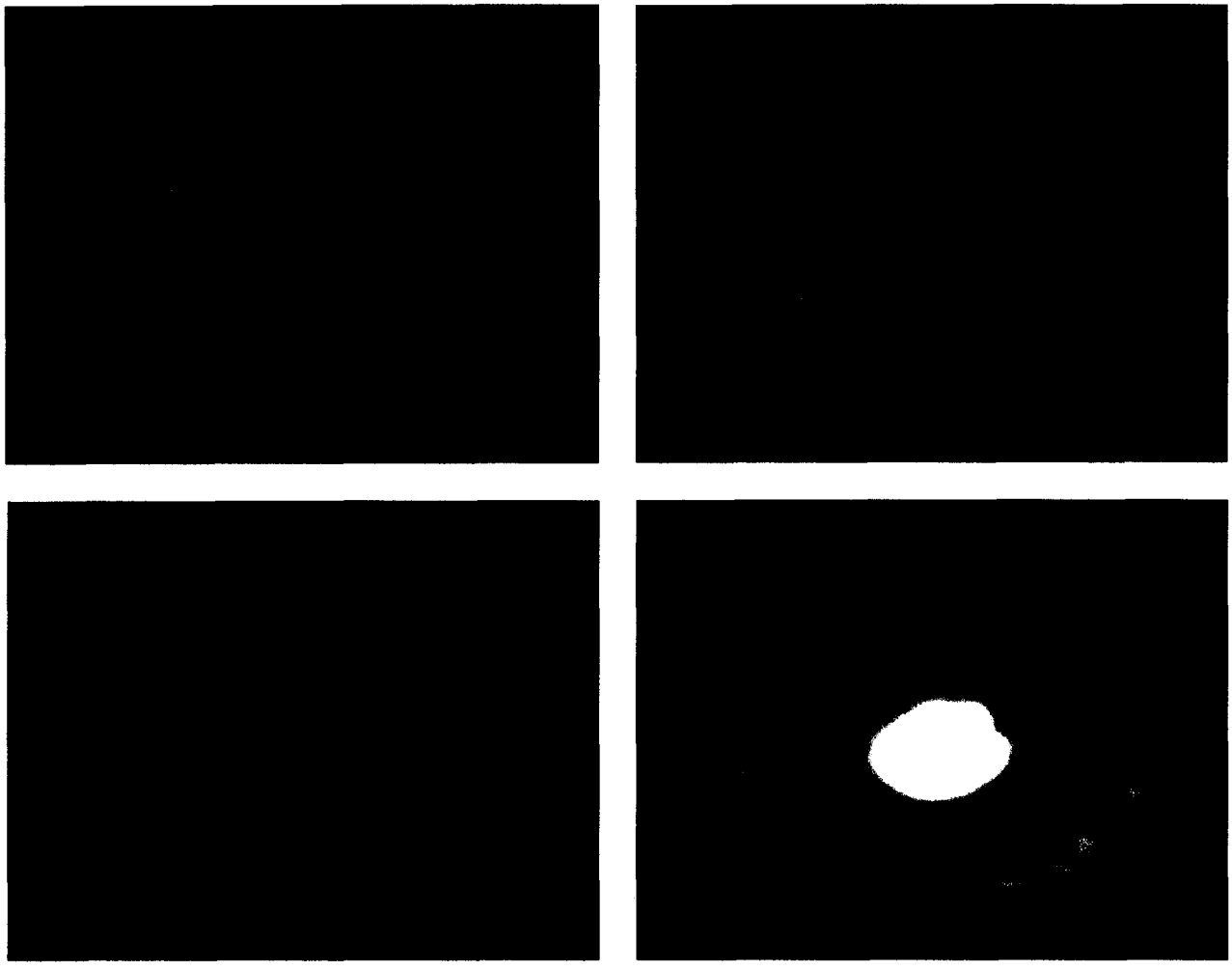

Figure 2. Typical reimaged Martian landmark maps

The maps themselves are built in a multi-step procedure:

1. Data is extracted from the images, rescaled and orthorectified based on the nominal landmark location, map coordinate frame, spacecraft locations, and camera orientations. The residuals between nominal and observed map space locations are translated into pixel-space residuals.

2. Images are registered (aligned), the central landmark vector determined, and (possibly) the spacecraft vectors found, by minimizing the mean square residuals between the predicted and observed image-space landmark locations.

3. The surface gradient and albedo at each pixelized location within the landmark are determined by minimizing the mean square residuals between the re-illuminated model and imaging data extracted from a number of pictures.

4. The gradients are integrated to produce the height distribution in the landmark, with either stereo points or MOLA data included to provide an absolute height scale, and to prevent errors in the gradient solutions from propagating too far.

These steps are discussed in the following four sections. Of necessity, the construction is iterative, with each step providing inputs for the others. Uncertainties in quantitied determined in each of the steps have minimal impact on the others, allowing the overall procedure to converge.

The final section discusses applications, including development of a net of navigation tie-points on Mars, the mapping and shape determination of small bodies, and the use of landmarks for autonomous body-relative navigation.

2. Image data extraction

A landmark is specified by a vector **V** from the center of a body fixed coordinate system to the origin of a local surface (map) coordinate system, by the axes of that coordinate system $\mathbf{u}_i$ (i=1,3), roughly in the south, east and vertical directions, and by heights and albedos at positions (x,y) relative to that system. The coordinates of a body-fixed point **P** on the surface are $x=\mathbf{u}_1\bullet(\mathbf{P}-\mathbf{V})$and $y=\mathbf{u}_2\bullet(\mathbf{P}-\mathbf{V})$ with the height $h(x,y)=\mathbf{u}_3\bullet(\mathbf{P}-\mathbf{V})$ and an albedo a(x,y). The camera geometry, its position vector **W** and its coordinate system $\mathbf{c}_i$ (i=1,3), unit vectors in the sample, line and boresight directions, respectively, are also specified in body-fixed coordinates.

For a simple narrow angle camera with focal length f, the image location X,Y on the focal plane of the point **P**(x,y,h) on the surface is given by

1a) $X = f(\mathbf{P}-\mathbf{W})\bullet\mathbf{c}_1/(\mathbf{P}-\mathbf{W})\bullet\mathbf{c}_3$

1b) $Y = f(\mathbf{P}-\mathbf{W})\bullet\mathbf{c}_2/(\mathbf{P}-\mathbf{W})\bullet\mathbf{c}_3$

which can be expanded to

2a) $X = f((\mathbf{V}-\mathbf{W})\bullet\mathbf{c}_1+M_{11}x+M_{12}y+M_{13}h)/((\mathbf{V}-\mathbf{W})\bullet\mathbf{c}_3+M_{31}x+M_{32}y+M_{33}h)$

2b) $Y = f((\mathbf{V}-\mathbf{W})\bullet\mathbf{c}_2+M_{21}x+M_{22}y+M_{23}h)/((\mathbf{V}-\mathbf{W})\bullet\mathbf{c}_3+M_{31}x+M_{32}y+M_{33}h)$

where $M_{ij}=\mathbf{c}_i\bullet\mathbf{u}_j$. The vector **V** to the origin of the landmark map specifies the body-fixed landmark location.

Initially, the heights are set equal to zero, turning the map into a flat piece of surface. For each (x,y) of the map, the corrosponding image locations (X,Y) are determined and the image data extracted. The maximum brightness values are stretched to full scale.

Figure 3 shows such a data extraction. The first two imaces are MOC data, and are relatively well aligned. The remaining Viking images are not yet regestered The maps are 100 km square (100x100 at 1 km resolution) to allow for an extended search area.

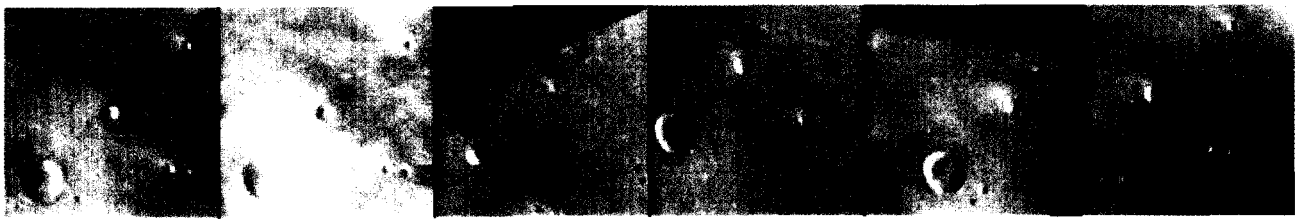

Figure 3. Initial data extraction for alignment of a landmark at 1 km resolution.

The map-space landmark locations translate directly into image space locations, with slight errors due to inaccuracies in camera pointing and landmark location. Once the rotough shift is accomplished, the resolution can be increased. The extracted data at 250 meter resolution is shown in figure 4.

Figure 4. Data extraction after alignment by hand at 250 meter resolution

From these data, and using the methods discussed in section 4, the surface slopes and albedos are determined, and the model reilluminated as in figure 5.

Figure 5. Reilluminated model of the landmark.

The reilluminated model is not as sharp as the original images. The bluring occurs because the original images are not accurately aligned. Nevertheless, the model is good enough to correlate with the corresponding image data to achieve alignment.

It is important to note that the data is extracted from a region surrounding the observed image space landmark locations, rather than a predicted locations based on estimates of camera geometry and landmark vector. Distortions can occur due to incorrect heights and errors in $M_{ij}=\mathbf{c}_i \bullet \mathbf{u}_j$.. As the landmark vector, camera geometry, slopes, albedos and heights are refined, the data extraction becomes sharper and the landmark modeling and alignment are improved.

For Mars, MOLA altimetry is a valuable addition to the optical data. Figure 6 show the reimaging of the 1/32 degree MOLA map [2] at 1 kilometer resolution. Although the imaging data can have better resolution, the MOLA data provides much a much better determination of landmark location than can be done with stereo alone.

Figure 6. Reillumination of MOLA data at 1 km resolution.

3. Camera and landmark geometry

The previous procedure provides a set of image space locations for a number of landmarks in a number of images. While it might be possible to do a multi-dimensional estimation for the locations of all the landmarks and the camera locations and orientations for all of the images, it is easier to iterate, alternately solving for each landmark's location and the camera geometry for each image..

If the ensemble of landmark vectors were known, as well as their locations (X,Y) in an image, then the camera orientation **c** and location **W** could be determined. Equations 2, or their equivalent for other imaging systems [3], predict the image space location of the landmark map origin as $X_p=X(\mathbf{W},\mathbf{c})$, $Y_p=Y(\mathbf{W},\mathbf{c})$ where **W** and **c** are the nominal values. The corrected values $\mathbf{W}+\delta\mathbf{W}$, $\mathbf{c}+\delta\mathbf{c}$ are determined by minimizing the function

3) $$C = \langle [(X_m - X_p - \delta\mathbf{W}\bullet\nabla_W X - \delta\mathbf{c}\bullet\nabla_c X)^2 + (Y_m - Y_p - \delta\mathbf{W}\bullet\nabla_W Y - \delta\mathbf{c}\bullet\nabla_c Y)^2]/\sigma^2 \rangle$$

where the average is over all landmarks in the image. $\delta\mathbf{W}$ stands for shifts in each of the components of **W** while $\delta\mathbf{c}$ stands for a rotation of the camera about each of its axes. X_m ,Y_m is the measured image space position of a given landmark, and σ contains the uncertainty in the landmark's image space location, due both to measurement uncertainties in X and Y, and to formal uncertainties in the landmark vector **V**.

The minimization of C is accomplished by setting its partials with respect to $\delta\mathbf{W}$ and $\delta\mathbf{c}$ equal to zero. This yields a set of six coupled linear equations of the form $\mathbf{Mv=w}$, where the information maxrix **M** is quadratic in the partials of X and Y, w is made up of products of those partials and the residuals, and the components of **v** are $\delta\mathbf{W}$ and $\delta\mathbf{c}$. The inverse of the information matrix, $\mathbf{M}^{-1}$, is the covarience matrix. Its diagonal elements measure the formal uncertainties σ^2 in the corresponding variables. To **M** should be added a diagonal apriori information matrix $\mathbf{M}_0$. In particular, if the camera position vector **W** is to be taken as a given, then large W-components in $\mathbf{M}_0$. will guarantee that $\delta\mathbf{W}$ is small, as will be the corresponding σ^2.

Similarly, if the camera geometry were known for the ensemble of images, as well as the locations (X,Y) of a landmark in those images, then the body-fixed vector V to that landmark could be determined., this time by solving a set of three coupled linear equations. The formal uncertainties in camera geometry coming from the solution above feed into the determination of **V**, just as its formal uncertainties feed into the determination of **c** and **W**.

Since there can be literally thousands of landmarks in thousands of images, a full-scale estimation would require the inversion of a matrix with dimension in the tens of thousands. By iterating the problem as above, it involves only the inversion of 3x3 or 6x6 information matrices.

4. Slope and albedo determination

If the landmarks are already aligned closely enough, to within a few percent of the size of the map, then the map projected brightness of the kth imagecan be fit to a simple function of slope and albedo

4) $I_k(x,y,\mathbf{t}) = \Lambda_k(1+t_3(x,y))F(\cos i,\cos e,g) + \Phi_k$

where F is an appropriate reflectance function [4,5]. A reasonable reflectance function seems to be 35% Lambert and 65% Lommel-Seeliger.

5) $F(\cos i,\cos e,g) = 0.35\cos i + 0.65\cos i/(\cos i+\cos e)$

No phase dependence has been included since only relative brightnesses are used and g is constant for a each image. Since during its extraction, the imaging data is maximally scaled., the multiplier Λ_k is included . Moreover, due to background or haze in some images, or perhaps because superresolution sampling has left a "washed out" look, a positive background term Φ_k can be added.

The factor $(1+t_3)$ is the relative albedo at map coordinates (x,y), normalized so that $\langle t_3\rangle=0$ over the map, g is the phase angle, i is the local angle of incidence and e is the local angle of emission. In terms of the (negative) slopes t_1=-dh/dx and t_2=-dh/dy, the local arguments of the function F are

6a) $\cos i = (s_1t_1+s_2t_2+s_3)/\sqrt{(1+t_1^2+t_2^2)}$

6b) $\cos e = (e_1t_1+e_2t_2+e_3)/\sqrt{(1+t_1^2+t_2^2)}$

where **s** and **e** are the map system components of the sun and spacecraft unit vectors respectively.

Each map is typically about a hundred pixels across. At each of these pixels (x,y), the values of t_i are solved for, fitting the extracted brightness data $E_k(x,y)$ to equation 4) by minimizing

7) $C = \langle(E_k(x,y) - I_k(x,y,\mathbf{t}) - \delta\mathbf{t}\bullet\nabla_t I_k(x,y,t))^2/\sigma^2\rangle$

where the average is over the images. The measurement uncertainty σ is determined from the brightness in the original image, as well as the values of Λ and Φ. The minimization results in the slope solution shown in figure 7. The left hand image represents north-south slopes, with a maximim of 0.33, and the right hand image shows the east-west slopes with maximum 0.24.

Figure 7. NS and EW slope solutions for the landmark.

The NS slopes in figure 7 are much grainier than the EW slopes. Moreover, the maximum slope is larger. Due to sun and spacecraft locations, the data is not very strong in the NS direction. The formal NS slope uncertainty is about 0.047, as opposed to the 0.007 for the EW slopes and 0.010 for the relative albedo. With such a weak NS slope signal, it is important to put a "tight apriori" on the albedo, so it doesn't have a chance to mask the slope information.

After determining the global factor Λ_k for each picture, and the additive constants Φ_k if appropriate, reconstructed images are made from the slope solutions using equations 4) and 5). These were shown in figure 4.

5. Height determination

In principal, the slopes determined from the minimization of (6) can be integrated to give a set of heights, provided that at least one starting height is known. There are three fundamental problems with this strategy. First, the slopes in the NS and EW directions are determined independently, without including the curl-free condition that $\partial_1 t_2 - \partial_2 t_1 = 0$. Second, the slopes have significant formal errors.. Finally, a starting height, or set of starting heights, is needed.

The curl-free condition follows automatically if a set of heights is determined, and is then used to determine slopes. The errors in the slopes are minimized by determining the height at a point by integrating from other "known" heights along multiple paths. If the height is known at the point (i-1,j) on the pixelized map, then the height at (i,j) is

7a) $h(i,j)=h(i-1,j)-(t_1(i-1,j)+t_1(i,j))s/2,$

where s is the pixel spacing. Similarly, if the height is known at (i,j-1), then

7b) $h(i,j)=h(i,j-1)-(t_2(i,j-1)+t_2(i,j))s/2.$

If more distant heights are known, then these too can give values for h(i,j), and several different paths can be used in the integration. In practice, the contributing heights are the eight, nearest and next-nearest neighbors, so that up tp twelve different combinations of slopes are integrated over and the resulting height solutions averaged.

For landmarks on Mars, the MOLA data provides a sparse set of initial heights. Points (i,j) are chosen at random, the slopes integrated from any known neighboring heights to the point of interest, and the results averaged to produce h(i,j). If the height at (i,j) is already known, then it is also included in the average. The process is repeated, randomly jumping from point to point to avoid spurious patterns that can result from using a fixed order.

In the absence of MOLA, stereo can be used to provide the initial heights. The distortions due to incorrect heights can be used to correct those heights at some points in the map. A small patch around (x,y) in a reconstruction such as figure 5 is correlated with the same patch of extracted data as the assumed height is varied. If a sufficiently strong peak is observed, then h(x,y) is taken to be the corresponding height. The number of heights determined in this way depends upon the complexity of the scene, and upon the original imaging geometry. For small bodies such as Phobos, heights sampled from neighboring maps can be used to provide the initial set. These maps evntually tile the body, defining its shape.

The heights determined from the integrations can be used to determine a new set of slopes such as those exhibited in figure 8. The maximum EW slope in the new solution is 0.22, close to the original value. The maximum NS slope has come down to a more consistent value of 0.25.

Figure 8. Slopes determined from the height solutions.

The heights themselves, along with the small albedo variations, are reilluminated in figure 9. The observer is at a 45 degree elevation, looking north, while the sun is 20 degrees above the eastern horizon. In a sense, the slope data determined from stereophotoclinometry has been used to interpolate the MOLA data, providing a much denser topography than the MOLA alone. The reimaging of the MOLA data alone is seen in figure 10.

DL0003 Lt=28.70N Ln=126.63W Rd=3392.32 Sz= 25 km

Figure 9. Illuminated landmark map referred to IAU94 coordinates.

DL0003 Lt=28.70N Ln=126.63W Rd=3392.10 Sz= 25 km

Figure 10. Illuminated 1/32 degree MOLA data.

6. Discussion

The map derived in the previous section represents a small patch of surface attached to a vector **V**. Aligning the predicted images generated from the map with data extracted from the images (Section 2) allows the estimates of **c**, **W**, and **V** itself to be improved (Section 3). The improved geometry knowledge allows for better pixel by pixel slope and albedo determinations (Section 4). This enables better height determination (Section 5), improving the map and enabling better data extraction and alignment.

As the number of landmarks increases, a tight rigid network of fixed surface points constrains the solutions for **c**, **W**, and **V**. In the particular case of Mars, large, low resolution landmark maps can be created directly from the MOLA data and aligned with the extracted imaging data. The landmark vector **V** can be taken as given in this situation, thereby reducing the uncertainties in solutions for camera geometry. Better knowledge of camera geometry produces better solutions for other, higher resolution landmarks.

A network of navigation maps for Mars is currently being developed. The maps are typically 100x100 pixels at about 500 meter resolution. They can be used to define the locations of surface features for imaging on future orbital missions, for approach navigation or for reconstruction of Viking Orbiter navigation. Larger, higher resolution maps can be used to study potential landing sites, such as the Melas site in figure 11, or as initial topographies for even higher resolution surface simulations [6].

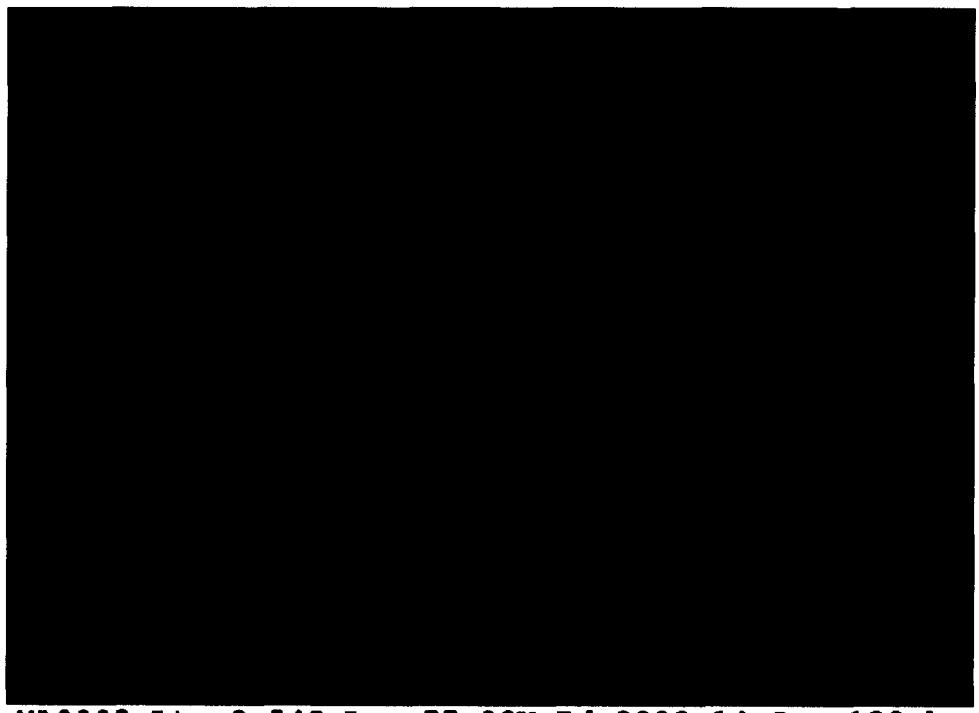

MA0002 Lt= 8.54S Ln= 77.92W Rd=3392.14 Sz= 128 km

Figure 11. A potential MER landing site.

If the approximate camera location and orientation is known, all potential landmarks in an image can rapidly be identified and data corresponding to the maps extracted. Figure 12 shows extracted and predicted landmarks for Viking orbiter image 629A39, the image presented at the beginning of this paper. The predictions and extractions are easily correlated and misalignments could easily be fed directly into autonomous onboard navigation software [7].

Figure 12. Extracted and predicted landmarks for Viking orbiter image 629A39.

Finally, for studies of small bodies, landmarks are used both as control points (figure 13a) and as larger maps which directly define the shape (figure 13b). Instead of a single stereo point, such a map provides tens of thousands of surface-defining vectors.

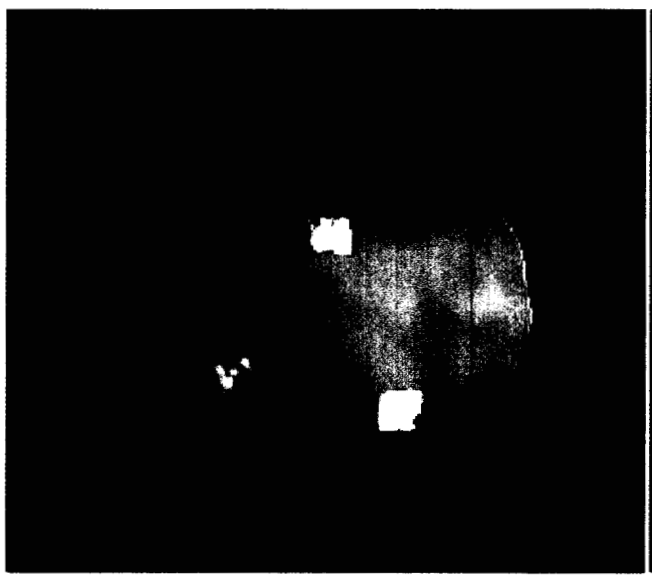

Figure 13a. Landmarks on Phobos

Figure 13b. Surace defining landmark map

Acknowledgements

This work was carried out at the Jet Propulsion Laboratory, California Institute of Technology, under a contract with the National Aeronautics and Space Administration.

References

[1] R. W. Gaskell, "Digital Identification of Cartographic Control Points," Photogrammetric Engineering and Remote Sensing 54, 723-727, Part 1, June 1988.

[2] "MOLA Topographic Map," http://wwwpds.wustl.edu/missions/mgs/mola/egdr.html

[3] B. Semenov, "MOC Instrument Kernel," FTP://NAIF/pub/naif/MGS/kernels/ik/moc20.ti, 2001.

[4] B. Hapke, "Bidirectional Reflectance Spectroscopy, I. Theory," Journal of Geophysical Research 86, 3039-3054, April, 1981.

[5] S. Squyres and J. Veverka, "Variation of Albedo with Solar-Incidence Angle on Planetary Surfaces," Icarus 50, 115-122, 1982.

[6] R. Gaskell, L. E. Husman, J. B. Collier and R. L. Chen, "Synthetic Environments for Simulated Missions," IEEE paper 13.0406, IEEE Aerospace Conference, Mar. 2001, Big Sky, Montana.

[7] R. Gaskell, "Automated Landmark Identification for Spacecraft Navigation," AAS paper 01-422, AAS/AIAA Astrodynamics Specialists Conf., August. 2001, Quebec City, PQ, Canada.